



**HAL**  
open science

## Density-tuned isotherms and dynamic change at phase transition in a gate-controlled superconducting system

Shamashis Sengupta, Miguel Monteverde, Anil Murani, Claire Marrache-Kikuchi, Andrés F Santander-Syro, Franck Fortuna

► **To cite this version:**

Shamashis Sengupta, Miguel Monteverde, Anil Murani, Claire Marrache-Kikuchi, Andrés F Santander-Syro, et al.. Density-tuned isotherms and dynamic change at phase transition in a gate-controlled superconducting system. 2021. hal-03157551v1

**HAL Id: hal-03157551**

**<https://hal.science/hal-03157551v1>**

Preprint submitted on 3 Mar 2021 (v1), last revised 6 Sep 2022 (v3)

**HAL** is a multi-disciplinary open access archive for the deposit and dissemination of scientific research documents, whether they are published or not. The documents may come from teaching and research institutions in France or abroad, or from public or private research centers.

L'archive ouverte pluridisciplinaire **HAL**, est destinée au dépôt et à la diffusion de documents scientifiques de niveau recherche, publiés ou non, émanant des établissements d'enseignement et de recherche français ou étrangers, des laboratoires publics ou privés.

# Density-tuned isotherms and dynamic change at phase transition in a gate-controlled superconducting system

Shamashis Sengupta,<sup>1,\*</sup> Miguel Monteverde,<sup>2</sup> Anil Murani,<sup>2</sup> Claire Marrache-Kikuchi,<sup>1</sup> Andrés F. Santander-Syro,<sup>3</sup> and Franck Fortuna<sup>3</sup>

<sup>1</sup>*Université Paris-Saclay, CNRS/IN2P3, IJCLab, 91405 Orsay, France*

<sup>2</sup>*Université Paris-Saclay, CNRS, Laboratoire de Physique des Solides, 91405, Orsay, France*

<sup>3</sup>*Université Paris-Saclay, CNRS, Institut des Sciences Moléculaires d'Orsay, 91405, Orsay, France*

Insights into the role of interactions in determining the macroscopic state of a system can be obtained by observing its evolution with an isothermal variation of density. We explore the isothermal evolution of the electron gas in  $\text{AlO}_x/\text{SrTiO}_3$  by a continuous gate-controlled tuning of its carrier density across the phase diagram exhibiting a superconducting dome. It is seen that condensation of the ordered phase leads to non-monotonic isotherms within the superconducting dome. The system undergoes dynamic change lasting tens of seconds following changes in gate voltage near the onset of the transition, revealing a strong impact of structural defects and distortions of the substrate on the superconducting state. These observations suggest that  $\text{AlO}_x/\text{SrTiO}_3$  is a promising platform to study time-dependent kinetic processes at the onset of superconductivity.

Understanding the evolution of the macroscopic state of a many-body-system with variation of particle number density is a topic of general interest in condensed matter physics. A large variety of solid-state systems exhibit a superconducting dome in the phase diagram. The key aspect of a superconducting dome is the non-monotonic variation of critical temperature ( $T_c$ ) as a function of carrier density ( $n$ ), accompanied by an absence of superconductivity in underdoped and overdoped regimes (Fig. 1a). Apart from unconventional superconductors [1] in which this feature is well-known, it has been seen in certain conventional superconductors [2–5], electron gases in oxide heterostructures [6–10] and atomically thin materials [11–13]. One of the main points of interest in experimentally exploring such a phase diagram is to study how the system evolves under a variation of the carrier density. However, it is not practically feasible to tune the carrier density continuously in most superconductors. Phase diagrams of bulk superconductors are studied by heating or cooling multiple samples with certain fixed values of carrier density (determined by chemical doping or modification of lattice structure with pressure). In gate-voltage-controlled systems, the carrier density  $n$  is usually stabilized at certain fixed values of the gate voltage  $V_g$  and the superconducting transition is induced by continuously varying the temperature. In other words, the phase transition is induced along an isochore (Fig. 1a) without changing  $n$ . The primary aim of this work is to probe the evolution of a superconducting system along a series of isotherms to study the impact of changes in electron density on the macroscopic state. The experiment reported here was conducted in an  $\text{AlO}_x/\text{SrTiO}_3$  heterostructure. Our first objective is to map isothermal changes in resistance as a function of electron density close to the top of the superconducting dome (marked by the temperature  $T_m$  in Fig. 1a). The second objective is to investigate non-equilibrium effects associated with the onset of superconductivity by measuring the stabi-

lization time ( $\tau$ ) for attainment of steady state following a rarefaction of the electron gas.

Isothermal evolution of a many-body-system with varying density highlights the role played by interparticle interactions in determining its physical properties. An illustrative example is provided by the van der Waals gas. Its phase diagram [14] is conventionally depicted as a set of pressure-volume ( $P - V$ ) isotherms (Fig. 1b). The van der Waals gas shares an apparent similarity with an electronic system exhibiting a superconducting dome. The microscopic mechanisms giving rise to a superconducting dome are prominent at intermediate carrier densities (between underdoped and overdoped regimes) at low temperatures. Similarly, for the van der Waals gas, the attractive interaction leading to the condensation of the liquid phase manifests itself at intermediate volumes below a certain critical temperature  $T_c$ . It leads to the development of non-monotonic isotherms (Fig. 1b) below  $T_c$ , with negative bulk modulus (positive  $\frac{dP}{dV}$ ) in region II and positive bulk modulus elsewhere (regions I and III). This comparison suggests that studying the superconducting system with an isothermal variation of density across the phase diagram may yield interesting insights into the phenomenon of the superconducting dome.

The  $\text{AlO}_x/\text{SrTiO}_3$  heterostructure used in our experiment was prepared by evaporating 2 nm of Al on the surface of a  $\text{SrTiO}_3$  crystal under ultra-high vacuum using a method described in Refs. 15, 16. The conducting 2DEG is created by the doping of Ti 3d levels [17]. (Further details are provided in Supplemental Material [18].) Transport measurements were carried out by contacting the 2DEG with ultrasonic wire-bonding (Fig. 1c). First, the four-probe resistance ( $R$ ) was measured as a function of the temperature ( $T$ ) for different values of the gate voltage ( $V_g$ ) allowing us to determine the  $V_g$  corresponding to the maximum critical temperature  $T_m$  of the dome. Fig. 1d shows the results when  $V_g$  is changed from higher to lower values (from 60 V to -60 V in steps of 10

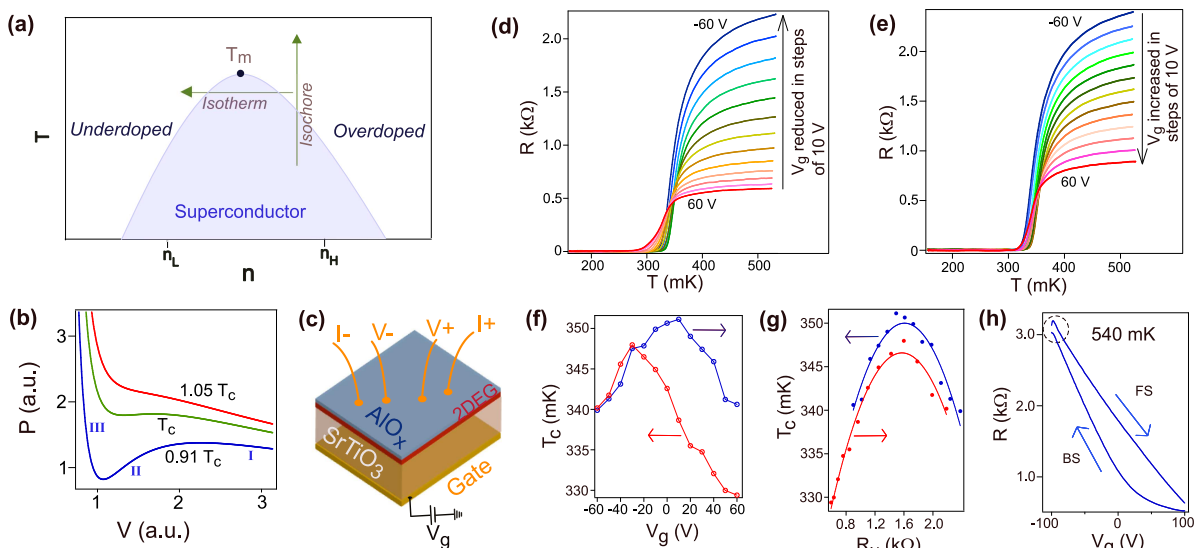


FIG. 1. (Color online) (a) Schematic of a superconducting dome phase diagram plotted as a function of temperature ( $T$ ) and carrier density ( $n$ ). The range of carrier densities accessible in our experiments (from  $n_L$  to  $n_H$ ) lies within the superconducting dome. (b) Pressure-Volume ( $P$ - $V$ ) isotherms simulated from the equation of state of a van der Waals gas close to the critical temperature  $T_c$ . (c) Schematic diagram of the heterostructure with wire bonded-contacts.  $I_+$ ,  $I_-$  are current leads and  $V_+$ ,  $V_-$  are voltage leads. (d, e) Four-probe resistance ( $R$ ) is measured as a function of temperature ( $T$ ) for different values of gate voltage  $V_g$ . The dc current applied is 20 nA. (f) The critical temperature  $T_c$  plotted as a function of  $V_g$ . Arrows indicate the chronological order in which the data, presented in (d) and (e), pertaining to these points was acquired. (g)  $T_c$  plotted as a function of  $R_N$  (the resistance at 500 mK). Solid lines are guides to the eye. (h) Resistance ( $R$ ) measured with a continuous variation of  $V_g$  (at a rate of 0.28 V/s). The current applied is 20 nA.

$V$ ), corresponding to a progressive lowering of the carrier density. Fig. 1e shows the set of curves for the reverse direction of change in  $V_g$ . (See Supplemental Material [18] for more results.) The critical temperature ( $T_c$ ) is defined to be the temperature where the slope of the superconducting resistance drop ( $\frac{dR}{dT}$ ) is maximum. The variation of  $T_c$  with  $V_g$  is shown in Fig. 1f. The domes for decreasing and increasing directions of gate voltages show a hysteresis with the maximum  $T_c$  appearing at different values of  $V_g$ . Hysteresis with changes in gate voltage may result from the presence of charged defects (mobile oxygen vacancies or charge traps) in the SrTiO<sub>3</sub> dielectric [9] and/or the time-dependent response of ferroic domains of the substrate to an applied electric field [19]. Such factors lead to different doping configurations for forward and backward sweeps of  $V_g$ . In Fig. 1g, the superconducting dome is represented as the variation of  $T_c$  with respect to the high-temperature resistance at 500 mK ( $R_N$ ). The maximum of  $T_c$  occurs for  $R_N \sim 1.5 - 1.6$  k $\Omega$  for both directions of change of  $V_g$ . This confirms that the relevant parameter for identifying the maximum critical temperature of the superconducting dome is indeed the carrier density. The result of a continuous tuning of  $V_g$  (at a sweep rate of 0.28 V/s), first in backward sweep (BS) and then in forward sweep (FS), is shown in Fig. 1h. In their study of the electron trapping mechanism in LaAlO<sub>3</sub>/SrTiO<sub>3</sub>, Yin et al. [20] observed that

electromigration and clustering of oxygen vacancies may give rise to an evolution of the 2DEG resistance for several seconds after the  $V_g$  has been stabilized following a ramp. We observe a similar effect in Fig. 1h (marked by a dashed circle).  $R$  increases with decreasing  $V_g$  during the BS, and continues to increase for a few seconds even after the  $V_g$  sweep direction is changed to FS. For all measurements reported in this paper, the sheet resistance (per square) can be obtained by multiplying the four-probe resistance by a factor of 3.2 (calculated from the geometry of the contacts). From Hall effect measurements at 4 K, the carrier density is found to be  $1.8 \times 10^{13}$  cm<sup>-2</sup> and  $2.9 \times 10^{13}$  cm<sup>-2</sup> for  $V_g$  of -80 V and 80 V respectively.

The result of isothermal tuning of carrier density is presented in Fig. 2. The gate voltage is tuned first in BS from 100 V to -100 V (Fig. 2a), then in FS from -100 V to +100 V (Fig. 2b) at a sweep rate of 0.28 V/s. At 395 mK, well above the onset of the macroscopic superconducting phase, we see the expected metallic behaviour of monotonic decrease (increase) in  $R$  with increase (decrease) in carrier density. At 325 mK, the evolution of  $R$  becomes non-monotonic with three distinct regions emerging (marked I, II, III). In region II,  $\frac{dR}{dn}$  is positive. Here, a reduction of the carrier density is accompanied by a reduction of the resistance. This non-monotonicity of the isotherm can be interpreted as a signature of the development of the superconducting

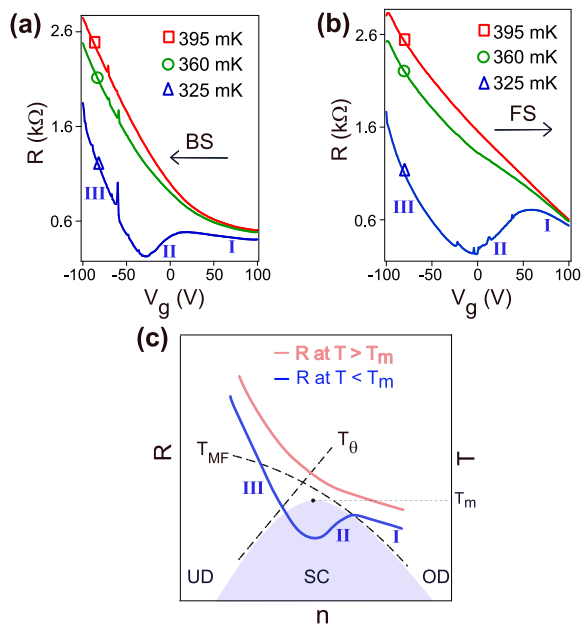


FIG. 2. (Color online) (a, b) The variation of resistance ( $R$ ) as a function of gate voltage ( $V_g$ ) at three different temperatures is shown for BS (a) and FS (b) respectively. The dc current applied was 20 nA. (c) Illustration of expected variation of resistance  $R$  (left-hand axis) as a function of carrier density  $n$  along isotherms of a system exhibiting a superconducting dome. The phase diagram with underdoped (UD), superconducting (SC) and overdoped (OD) regimes is represented with temperature  $T$  along the right-hand axis.

phase. A prototypical system with a superconducting dome (Fig. 2c) is composed of weakly interacting carriers in the overdoped regime (with large carrier density  $n$ ). As  $n$  is progressively reduced at constant temperature (below  $T_m$  of the dome), first there is an augmentation of the mean-field superconducting gap followed by a gradual loss of phase coherence towards lower densities in the underdoped regime. In Fig. 2c, the line  $T_{MF}$  denotes schematically the mean-field transition temperature and  $T_\theta$  denotes the upper bound on the phase ordering temperature (following the theoretical work by Emery and Kivelson [21]). In the overdoped and underdoped regimes, outside the superconducting dome, the system is expected to show the characteristic of a normal conductor with negative  $\frac{dR}{dn}$ . This corresponds to regions I and III of the  $R - n$  isotherm for  $T < T_m$ . At intermediate densities, due to the formation of finite superfluid density within the superconducting dome, there is a deviation from this behaviour marked by a sharp drop in resistance. This causes the change in slope with positive  $\frac{dR}{dn}$  in region II of the isotherm.

We will now discuss about the measurement of dynamic changes of the 2DEG resistance following a gate-induced change in carrier density. The gate voltage is ramped from high to low  $V_g$  at a rate of 0.28 V/s, pro-

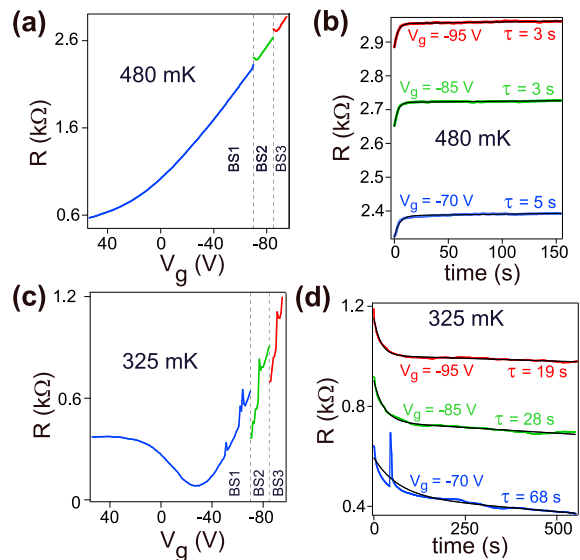


FIG. 3. (Color online) (a,b)  $V_g$  is swept at a rate of 0.28 V/s with progressive depletion of the electron gas at 480 mK. (a) shows the ensuing change in  $R$ . Three sets of measurements are shown, with  $V_g$  sweep terminating at -70 V (BS1), -85 V (BS2) and -95 V (BS3). The  $V_g$ -axis is plotted to correspond with increasing time from left to right. Dynamic change in  $R$  upon stopping the  $V_g$  sweep is shown in (b). The dc current applied is 20 nA. (c,d) The same experimental protocol described in (a,b) is followed, at a temperature of 325 mK. Variation of  $R$  during  $V_g$  sweep is shown in (c). Dynamic change in  $R$  after  $V_g$  is stabilized is shown in (d).

gressively reducing  $n$ , before it is stopped at a certain value of  $V_g$  (where it is thereafter held steady). The resistance  $R$  is then monitored with time  $t$ . This set of measurements is performed at 480 mK (Figs. 3a and 3b) and 325 mK (Figs. 3c and 3d), stopping the  $V_g$  ramp at values of -70 V, -85 V and -95 V. At 480 mK, the resistance becomes steady after a few seconds (Fig. 3b). This observation can be explained as an effect of the motion of charged defects within the bulk substrate (as mentioned earlier). Upon lowering the temperature to 325 mK, the dynamic change with time becomes quite different. Instead of an increase in  $R$ , we observe a larger reduction in  $R$  (Fig. 3d). More importantly, the evolution takes place over a much longer time before an almost steady state is reached (Fig. 3d). At  $V_g = -70$  V, even after 500 seconds of wait,  $R$  still continues to reduce with time, showing that the time to reach a steady state is even longer. To quantify the characteristic timescales, we fit the data in Figs. 3b and 3d to the function  $R(t) = R_0 + \alpha e^{-t/\tau} + \beta t$  with  $R_0$ ,  $\alpha$ ,  $\beta$  and  $\tau$  as fit parameters. The final term  $\beta t$  accounts for the gradual change in resistance at large  $t$ . The term  $\alpha e^{-t/\tau}$  captures the sharp change in resistance just after  $t=0$  with a characteristic time  $\tau$ .  $\tau$  is found to be 5 s, 3 s, 3 s for  $V_g$  values of -70 V, -85 V, -95 V respectively at 480 mK (Fig. 3b). At 325 mK (below  $T_m$  of the superconducting dome), these increase to

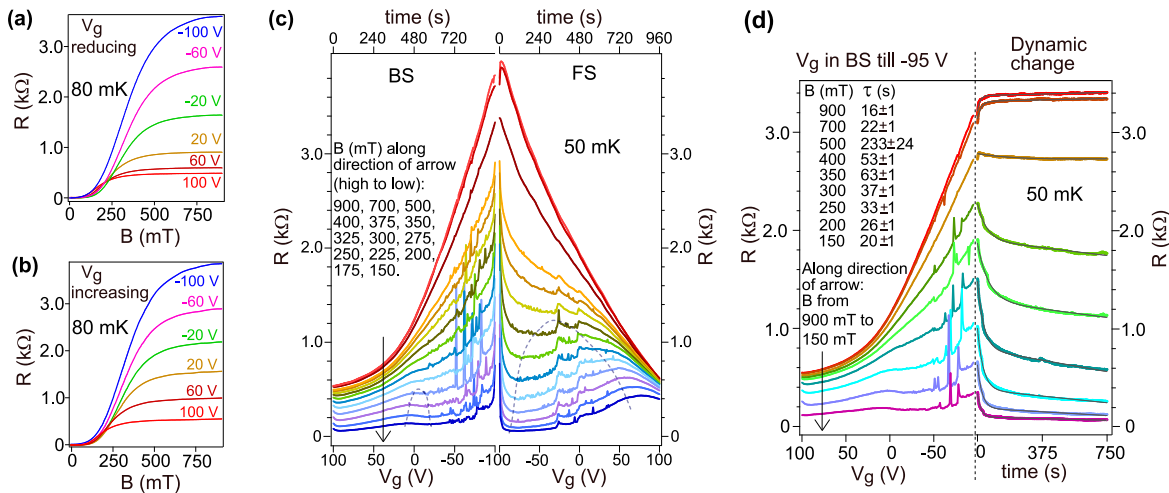


FIG. 4. (**Color online**) (a,b)  $R$  is measured as a function of magnetic field ( $B$ ) for different values of gate voltage  $V_g$  at 80 mK temperature. The current used was 20 nA in (a) and 100 nA in (b). (c)  $R$  is measured as a function of  $V_g$  at different values of the magnetic field  $B$  at 50 mK.  $V_g$  is first swept in back sweep (BS) and then in forward sweep (FS) at 0.21 V/s. Time increases from left to right. DC current applied is 50 nA. Dashed lines correspond to regions where  $\frac{dR}{dn}$  is positive. (d)  $V_g$  is swept at 0.21 V/s from 100 V to -95 V with progressive depletion of the electron gas at different values of  $B$  (left of dotted line) at 50 mK temperature. Then  $V_g$  is stabilized and dynamic change in  $R$  is recorded with time (right of the dotted line). Solid lines are fits to the data. DC current used is 10 nA.

68 s, 28 s and 19 s respectively (Fig. 3d). The increase in  $\tau$  appears to be directly related to the development of the superconducting phase. To cross-check this inference, we repeated these measurements by inducing the superconducting transition with a magnetic field.

The evolution of 2DEG resistance as a function of the magnetic field  $B$  was measured for different fixed values of  $V_g$  (Figs. 4a and 4b). We then measured the evolution of resistance with a continuous tuning of  $V_g$  at different values of  $B$ , with the temperature at 50 mK. These isolines of constant magnetic field are shown in Fig. 4c.  $V_g$  was first changed in BS from 100 V to -100 V, then in FS from -100 V to 100 V (at a sweep rate of 0.21 V/s). A clear difference is observed between the curves for BS and FS. A rapid drop in  $R$  is seen at the beginning of the FS, for field values below 400 mT. At low fields, a prominent region of positive  $\frac{dR}{dn}$  appears (indicated by a dashed curve) during forward  $V_g$  sweeps. This region is however barely visible in backward  $V_g$  sweep. This difference, we may infer, is related to the kinetics of the superconducting state. The microscopic configuration of the superconducting electronic system evolves differently during the introduction of carriers (FS) as compared to the depletion of carriers (BS). The electronic system is likely to be composed [7, 22, 23] of several superconducting islands. The degree of phase coherence between these islands determines the extent of macroscopic order. The rapid drop in  $R$ , seen at the beginning of the FS in Fig. 4c for field values less than 400 mT, suggests the formation of large phase coherent superconducting droplets upon the reversal of sweep direction of  $V_g$ . (See Sup-

plemental Material [18] for the outcome of varying  $V_g$  sweep rates.) As we will discuss now, the development of superconducting islands may be strongly influenced by intrinsic properties of the SrTiO<sub>3</sub> dielectric.

The dynamic change of  $R$  for attainment of steady state is measured by first ramping  $V_g$  down till -95 V (at 0.21 V/s) and recording the ensuing temporal evolution (Fig. 4d). At high fields,  $R$  increases for a certain time ( $\tau$  of 16 s at 900 mT and 22 s at 700 mT) before stabilizing at a steady value. At 500 mT, a different behaviour sets in. There is a momentary increase in  $R$  followed by a slow drop over an extended period of time.  $\tau$  is estimated to be 233 s. (See Supplemental Material [18] for further discussions.) At lower fields,  $R$  drops by larger amounts when the  $V_g$  sweep is stopped at -95 V. The noticeable difference of dynamic change behaviour at high and low fields can be explained by the fact that the low field behaviour is determined by the kinetics of superconducting islands. The resistance drop corresponds to the condensation or the increase in size of such islands. These estimated times of several seconds are difficult to explain in terms of a purely electronic mechanism. Such large timescales are possibly related to the properties of the SrTiO<sub>3</sub> substrate hosting the 2DEG. It is known that relaxation processes due to movement of oxygen vacancies inside SrTiO<sub>3</sub>, upon the application of an electric field [20] or ultra-violet radiation [24], may last for several seconds or even minutes. The motion of such charged defects under an electric field in our system can account for the observed values of  $\tau$  in the high temperature (Fig. 3b) or high-field (Fig. 4d) normal state. The moving de-

fects may provide a fluctuating potential landscape for the electrons, affecting the nucleation of superconducting droplets or the expansion of phase coherent superconducting islands. A small increase in the fraction of superconducting electrons will result in a significant reduction of the resistance. Accordingly, the dynamic change in resistance will be larger in magnitude and appreciable over a longer span of time with the onset of superconductivity. Another phenomenon of interest in understanding the large values of  $\tau$  is the existence of ferroic domains within SrTiO<sub>3</sub>. The impact of structural domains of SrTiO<sub>3</sub> on the properties of the conducting electronic system at the surface has been observed with scanning probe microscopy [25–27] and transport experiments [28]. Pesquera et al. [19] demonstrated that polar domains in SrTiO<sub>3</sub> under an applied electric field exhibit relaxation times of several tens of minutes at 36 K (the lowest temperature at which these experiments were conducted). Therefore, the large  $\tau$  observed in our experiments may also be related to the relaxation of structural domains within the dielectric and their influence upon the superconducting state. These observations may help to explain the spike-like features in the resistance of the 2DEG seen in Figs. 3d, 4c and 4d. These can result from sudden transformations in the arrangement of trapped charges or ferroic domains within the substrate, which influence the properties of the interface electronic system. It is noteworthy that such spike-like features in resistance are visible only at temperature and magnetic field values low enough for the onset of superconductivity to have taken place. These are not visible in the normal state, corroborating our inference that the 2DEG in AlO<sub>x</sub>/SrTiO<sub>3</sub> is much more sensitive to structural defects/deformations of the substrate in the superconducting state than in the normal state.

We have explored the superconducting dome in an AlO<sub>x</sub>/SrTiO<sub>3</sub> heterostructure by continuously varying its carrier density with a gate voltage  $V_g$  and measuring the evolution of resistance  $R$ . The  $R$ - $V_g$  isotherms are observed to be non-monotonic below the maximum critical temperature of the superconducting dome due to the non-monotonic variation of superfluid density as a function of carrier density. Dynamic change of tens of seconds is observed following a change of gate voltage close to the phase transition, highlighting the sensitivity of the superconducting state to structural defects and deformations of the underlying substrate. The large timescales make AlO<sub>x</sub>/SrTiO<sub>3</sub> a unique platform to study the real-time kinetics of the growth of the ordered superconducting state. Experiments with scanning probe microscopy on the superconductor NbTiN have revealed large timescales for fluctuations near criticality [29]. Probing AlO<sub>x</sub>/SrTiO<sub>3</sub> with such techniques may yield interesting results. Transport experiments on ultra-thin superconductors [11–13] with gate-voltage-tuning of carrier density, as outlined in this work, may yield fur-

ther new insights about the kinetics of superconductivity in low dimensions.

The authors thank R. Deblock, H. Bouchiat, S. Guéron and P. Senzier for help during the experiments. We thank D. Petrov for insightful discussions. This work was supported by public grants from the French National Research Agency (ANR), project CP-Insulators No. ANR-2019-CE30-0014-03.

---

\* sengupta@ijclab.in2p3.fr

- [1] B. Keimer, S. A. Kivelson, M. R. Norman, S. Uchida, and J. Zaanen, *Nature* **518**, 179 (2015).
- [2] J. F. Schooley, W. R. Hosler, E. Ambler, J. H. Becker, M. L. Cohen, and C. S. Koonce, *Phys. Rev. Lett.* **14**, 305 (1965).
- [3] X. Lin, G. Bridoux, A. Gourgout, G. Seyfarth, S. Krämer, M. Nardone, B. Fauqué, and K. Behnia, *Phys. Rev. Lett.* **112**, 207002 (2014).
- [4] S. Deemyad and J. S. Schilling, *Phys. Rev. Lett.* **91**, 167001 (2003).
- [5] K. Shimizu, T. Kimura, S. Furomoto, K. Takeda, K. Kontani, Y. Onuki, and K. Amaya, *Nature* **412**, 316 (2001).
- [6] A. D. Caviglia, S. Gariglio, N. Reyren, D. Jaccard, T. Schneider, M. Gabay, S. Thiel, G. Hammerl, J. Mannhart, and J.-M. Triscone, *Nature* **456**, 624 (2008).
- [7] J. Biscaras, N. Bergeal, S. Hurand, C. Feuillet-Palma, A. Rastogi, R. C. Budhani, M. Grilli, S. Caprara, and J. Lesueur, *Nature Materials* **12**, 542 (2013).
- [8] A. Joshua, S. Pecker, J. Ruhman, E. Altman, and S. Ilani, *Nature Communications* **3**, 1129 (2012).
- [9] C. Bell, S. Harashima, Y. Kozuka, M. Kim, B. G. Kim, Y. Hikita, and H. Y. Hwang, *Phys. Rev. Lett.* **103**, 226802 (2009).
- [10] D. A. Dikin, M. Mehta, C. W. Bark, C. M. Folkman, C. B. Eom, and V. Chandrasekhar, *Phys. Rev. Lett.* **107**, 056802 (2011).
- [11] J. T. Ye, Y. J. Zhang, R. Akashi, M. S. Bahramy, R. Arita, and Y. Iwasa, *Science* **338**, 1193 (2012).
- [12] L. J. Li, E. C. T. O’Farrell, K. P. Loh, G. Eda, B. Özyilmaz, and A. H. Castro Neto, *Nature* **529**, 185 (2016).
- [13] Y. Cao, V. Fatemi, S. Fang, K. Watanabe, T. Taniguchi, E. Kaxiras, and P. Jarillo-Herrero, *Nature* **556**, 43 (2018).
- [14] E. Fermi, *Thermodynamics*, Dover publications (1956).
- [15] S. Sengupta, E. Tisserond, F. Linez, M. Monteverde, A. Murani, T. Rödel, P. Lecoeur, T. Maroutian, C. Marrache-Kikuchi, A. F. Santander-Syro, and F. Fortuna, *J. Appl. Phys.* **124**, 213902 (2018).
- [16] T. C. Rödel, F. Fortuna, S. Sengupta, E. Frantzeskakis, P. L. Fèvre, F. Bertran, B. Mercey, S. Matzen, G. Agnus, T. Maroutian, P. Lecoeur, and A. F. Santander-Syro, *Advanced Materials* **28**, 1976 (2016).
- [17] A. F. Santander-Syro, O. Copie, T. Kondo, F. Fortuna, S. Pailhès, R. Weht, X. G. Qiu, F. Bertran, A. Nicolaou, A. Taleb-Ibrahimi, P. Le Fèvre, G. Herranz, M. Bibes, N. Reyren, Y. Apertet, P. Lecoeur, A. Barthélémy, and M. J. Rozenberg, *Nature* **469**, 189 (2011).

- [18] See Supplemental Material.
- [19] D. Pesquera, M. A. Carpenter, and E. K. H. Salje, *Phys. Rev. Lett.* **121**, 235701 (2018).
- [20] C. Yin, A. E. M. Smink, I. Leermakers, L. M. K. Tang, N. Lebedev, U. Zeitler, W. G. van der Wiel, H. Hilgenkamp, and J. Aarts, *Phys. Rev. Lett.* **124**, 017702 (2020).
- [21] V. J. Emery and S. A. Kivelson, *Nature* **374**, 434 (1995).
- [22] Z. Chen, A. G. Swartz, H. Yoon, H. Inoue, T. A. Merz, D. Lu, Y. Xie, H. Yuan, Y. Hikita, S. Raghu, and H. Y. Hwang, *Nature Communications* **9**, 4008 (2018).
- [23] G. E. D. K. Prawiroatmodjo, F. Trier, D. V. Christensen, Y. Chen, N. Pryds, and T. S. Jespersen, *Phys. Rev. B* **93**, 184504 (2016).
- [24] S. Suwanwong, T. Eknapakul, Y. Rattanachai, C. Masingboon, S. Rattanasuporn, R. Phatthanakun, H. Nakajima, P. D. C. King, S. K. Hodak, and W. Meevasana, *Applied Surface Science* **355**, 210 (2015).
- [25] B. Kalisky, E. M. Spanton, H. Noad, J. R. Kirtley, K. C. Nowack, C. Bell, H. K. Sato, M. Hosoda, Y. Xie, Y. Hikita, C. Woltmann, G. Pfanzelt, R. Jany, C. Richter, H. Y. Hwang, J. Mannhart, and K. A. Moler, *Nature Materials* **12**, 1091 (2013).
- [26] M. Honig, J. A. Sulpizio, J. Drori, A. Joshua, E. Zeldov, and S. Ilani, *Nature Materials* **12**, 1112 (2013).
- [27] H. Noad, E. M. Spanton, K. C. Nowack, H. Inoue, M. Kim, T. A. Merz, C. Bell, Y. Hikita, R. Xu, W. Liu, A. Vailionis, H. Y. Hwang, and K. A. Moler, *Phys. Rev. B* **94**, 174516 (2016).
- [28] Y.-Y. Pai, H. Lee, J.-W. Lee, A. Annadi, G. Cheng, S. Lu, M. Tomczyk, M. Huang, C.-B. Eom, P. Irvin, and J. Levy, *Phys. Rev. Lett.* **120**, 147001 (2018).
- [29] A. Kremen, H. Khan, Y. L. Loh, T. I. Baturina, N. Trivedi, A. Frydman, and B. Kalisky, *Nature Physics* **14**, 1205 (2018).

# Supplemental Material: Density-tuned isotherms and dynamic change at phase transition in a gate-controlled superconducting system

Shamashis Sengupta,<sup>1</sup> Miguel Monteverde,<sup>2</sup> Anil Murani,<sup>2</sup> Claire Marrache-Kikuchi,<sup>1</sup> Andrés F. Santander-Syro,<sup>3</sup> and Franck Fortuna<sup>3</sup>

<sup>1</sup>*Université Paris-Saclay, CNRS/IN2P3, IJCLab, 91405 Orsay, France*

<sup>2</sup>*Université Paris-Saclay, CNRS, Laboratoire de Physique des Solides, 91405, Orsay, France*

<sup>3</sup>*Université Paris-Saclay, CNRS, Institut des Sciences Moléculaires d'Orsay, 91405, Orsay, France*



## 1. Fabrication of $\text{AlO}_x/\text{SrTiO}_3$ heterostructure

The  $\text{AlO}_x/\text{SrTiO}_3$  heterostructure was prepared using a commercially available (001)-oriented  $\text{SrTiO}_3$  crystal (measuring 5 mm x 5 mm x 0.5 mm). The  $\text{SrTiO}_3$  crystal was placed inside an UHV (ultrahigh vacuum) chamber. An annealing step was performed to clean the surface contamination. The sample was heated to 600°C for 1 minute. Then the temperature was allowed to reduce, and 2 nm of Al was evaporated using a Knudsen cell at a temperature higher than room temperature (200° C). The rate of deposition of Al was 0.002 nm/s. This produces an  $\text{AlO}_x/\text{SrTiO}_3$  heterostructure with a conducting electron gas at the interface. The backplane of the  $\text{SrTiO}_3$  crystal was glued to a copper plate with conductive silver paint to serve as the gate electrode. The resistance of the  $\text{SrTiO}_3$  substrate between the surface with 2DEG and the gate electrode is greater than 100 G $\Omega$ .

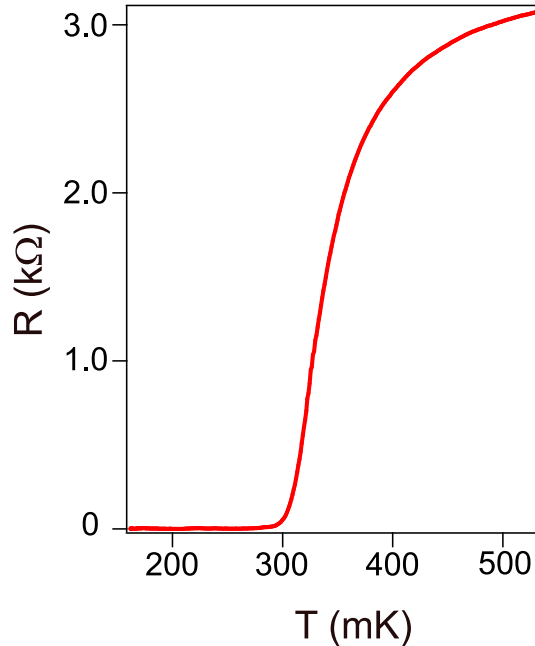


FIG. S1. Variation of resistance ( $R$ ) as a function of temperature ( $T$ ) at a gate voltage of -100 V. The current applied was 20 nA. The critical temperature (defined as the point of maximum slope  $\frac{dR}{dT}$ ) is 324 mK.

## 2. Superconducting transition at a gate voltage of -100 V

We have presented data in the main text (Fig. 3d) of a significant reduction in resistance with time when the gate voltage sweep is stopped at  $V_g$  values of -70 V, -85 V and -95

V. This measurement was done at 325 mK. The resistance measured is finite because this temperature is still above the temperature at which resistance becomes zero. The variation of resistance showing the full superconducting transition as a function of temperature, at a fixed gate voltage of -100 V, is shown in Fig. S1.

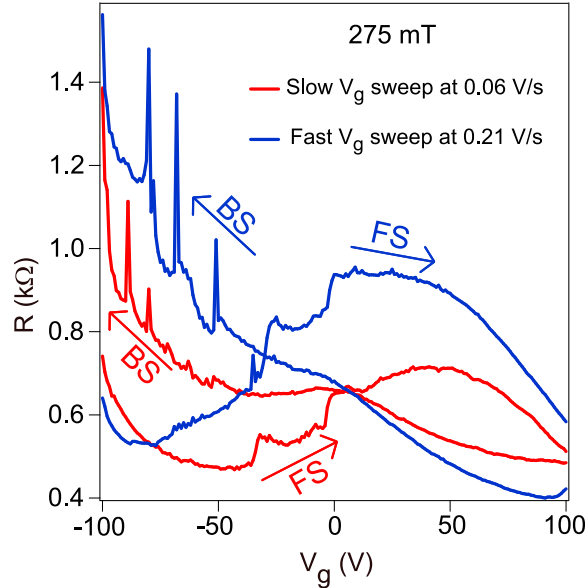


FIG. S2. Variation of resistance ( $R$ ) with gate voltage ( $V_g$ ) sweep. The temperature is 50 mK and applied magnetic field is 275 mT. The experimental protocol is the following.  $V_g$  is ramped from 0 V to 100 V (not shown). Then, it is reduced in backsweep (BS) from 100 V to -100 V.  $V_g$  is held at -100 V for two minutes and then swept back to 100 V in forward sweep (FS). This set of measurements is carried out for two different  $V_g$  sweep rates. The DC current used is 10 nA.

### 3. The result of variation of gate voltage sweep rate on the evolution of resistance

In the main text, we identified two possible causes for the large timescales in dynamic change behaviour of the resistance  $R$  following a continuous change of the gate voltage  $V_g$  near the onset of superconductivity. These were the motion of charged defects (primarily oxygen vacancies) within the bulk dielectric, and the relaxation of ferroic domains in the substrate. Both of these are known to exhibit dynamics lasting several seconds. Given this explanation, one can expect that a variation of the sweep rate will result in visible changes in the evolution of resistance. This experiment is shown in Fig. S2.  $V_g$  was swept in both back sweep (BS) and forward sweep (FS) at 50 mK temperature with an applied magnetic

field of 275 mT. Two different sweep rates were used: 0.21 V/s (fast) and 0.06 V/s (slow). The overall variation of  $R$  is clearly less for the slower  $V_g$  sweep in comparison to the faster one.

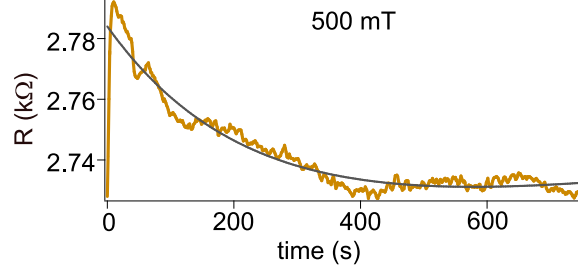


FIG. S3. This plot is reproduced from Fig. 4d of the main text for clarity. It shows the dynamic change of resistance  $R$  with time  $t$  at 500 mT after the gate voltage sweep is stopped at -95 V.

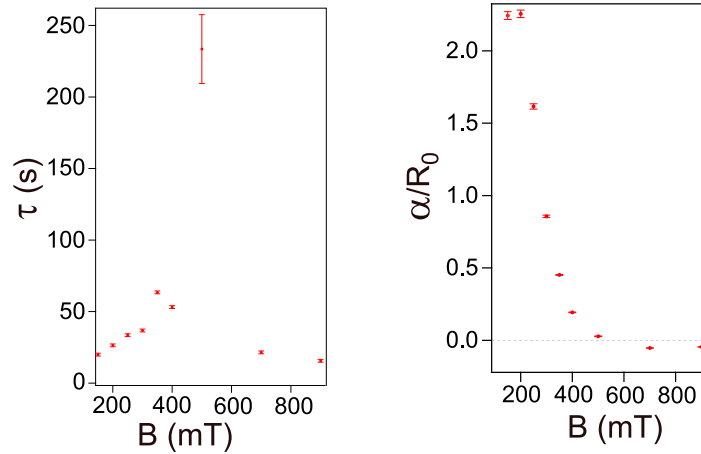


FIG. S4. The estimated values of  $\tau$  and  $\alpha/R_0$  from the dataset in Fig. 4d of main text.

#### 4. Dynamic change of resistance at different magnetic fields

The dynamic change of resistance  $R$  of the 2DEG following a sweep of the gate voltage was studied at different magnetic fields and the data was presented in Fig. 4d of the main text. The data was fitted to the function  $R(t) = R_0 + \alpha e^{-t/\tau} + \beta t$ .  $\tau$  is the characteristic time over which the sharp change in  $R$  occurs once the gate voltage value is stabilized at -95 V.  $\alpha$  is the magnitude of this drop (with the fractional change given by  $\alpha/R_0$ ). As the magnetic field is progressively reduced starting from 900 mT, a huge increase in  $\tau$  is

observed at 500 mT. The plot showing the dynamic change of  $R$  at 500 mT is shown in Fig. S3. This is the same plot as shown in Fig. 4d of main text - it is reproduced here for clarity.  $R$  continues to increase for the initial 10 seconds, after which the trend reverses and a gradual reduction in  $R$  begins. The estimated values of  $\tau$  and  $\alpha/R_0$  for the different values of magnetic field (from the dataset in Fig. 4d of main text) are shown in Fig. S4.

---